ACS Catalysis

pubs.acs.org/acscatalysis

Research Article

Structural and Mechanistic Insights into Chain Release of the Polyene PKS Thioesterase Domain

Yucong Zhou, Wentao Tao, Zhen Qi, Jianhua Wei, Ting Shi, Qianjin Kang, Jianting Zheng,* Yilei Zhao,* and Linquan Bai*

Cite This: *ACS Catal.* 2022, 12, 762−776

Read Online

ACCESS | Metrics & More | Article Recommendations | Supporting Information

ABSTRACT: Polyketides serve as rich source of therapeutically relevant drug leads. The manipulation of polyketide synthases (PKSs) for generating derivatives with improved activities usually results in substantially reduced yields. Growing evidence suggests that type I PKS thioesterase (TE) domains are key bottlenecks in the biosynthesis of polyene antibiotics, such as pimaricin and amphotericin, and their unnatural derivatives. Herein, we elucidate the structure of the 26-membered macrolide-complexed TE domain from the pimaricin pathway (Pim TE), which specifies a spacious bifunnel-shaped substrate channel with a highly hydrophobic cleft proximal to the catalytic triad and a hydrophilic loop I region specific for the cyclization of amphiphilic polyene macrolide. Notably, the natural intermediate with C12-COOH is stabilized by a hydrogen-bond network, as well as by interactions between the polyene moiety and the hydrophobic cleft. Moreover, the bottleneck in processing the unnatural intermediate with C12-CH_3 is attributed to the unstable and mismatched docking of the curved substrate in the channel. Aided by an *in vitro* assay with a fully elongated linear polyene intermediate as the substrate, multiple strategies were adopted, herein, to engineer Pim TE, including introducing H-bond donors, enhancing hydrophobic interactions, and modifying the catalytic center. Efficient TE mutations with increased substrate conversion up to 39.2% *in vitro* were further conducted *in vivo*, with a titer increase as high as 37.1% for the less toxic decarboxylated pimaricin derivatives with C12-CH_3. Our work uncovers the mechanism of TE-catalyzed polyene macrolide formation and highlights TE domains as targets for PKS manipulation for titer increases in engineered unnatural polyketide derivatives.

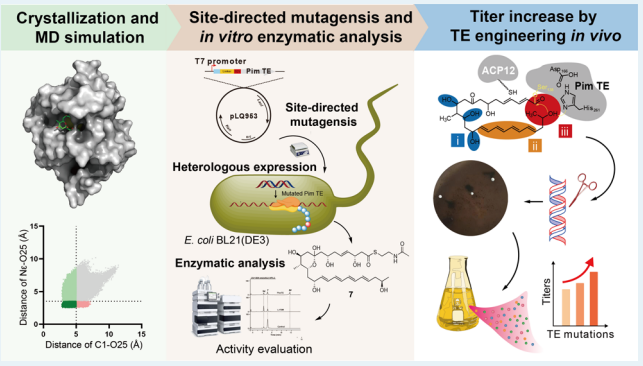

KEYWORDS: *polyene antibiotics, polyketide synthases, thioesterase domain, chain release, structural biology*

INTRODUCTION

Polyketides often serve as lead compounds for improving biological properties by medicinal chemistry;[1] however, cell toxicity, drug resistance, water solubility, and stability often present challenges for drug development.[2] The biosynthetic machinery of microbial polyketide natural products has evolved delicately with specific recognition and efficient catalysis of upstream intermediates by downstream enzymes/domains.[3] Therefore, manipulations of polyketide synthases (PKSs) and their related tailoring enzymes usually cause attenuated production or abolish the accumulation of intermediates with modified structures.[4−6]

Type I modular PKS is considered one of the most well-studied biosynthetic systems to catalyze a series of stepwise condensations of small and simple acyl-CoA building blocks.[7] Typically, in type I PKSs, each module catalyzes an elongation step on the nascent polyketide chain that requires a minimal set of three domains: (i) an acyltransferase (AT) domain that selects and loads the appropriate extender unit onto an acyl carrier protein (ACP) domain; (ii) an ACP domain tethered with a 4′-phosphopantetheine arm to bind the growing polyketide chain; and (iii) a ketosynthase (KS) domain that catalyzes a decarboxylative Claisen condensation to fuse the acyl moiety and the extender unit. In addition, three domains are optionally present in PKSs, which successively reduces the *β*-keto group to a hydroxy (ketoreductase domain; KR), a hydroxy to a double bond (dehydratase domain; DH), and a double bond to methylene (enoylreductase domain; ER). Generally, there is a thioesterase (TE) domain at the C-terminal of PKSs, such as those for erythromycin,[8] avermectin,[9] and amphotericin[10] biosynthesis, which are responsible for the polyketide chain release by intramolecular cyclization or direct hydrolysis.

Received: October 30, 2021
Revised: December 12, 2021
Published: December 28, 2021

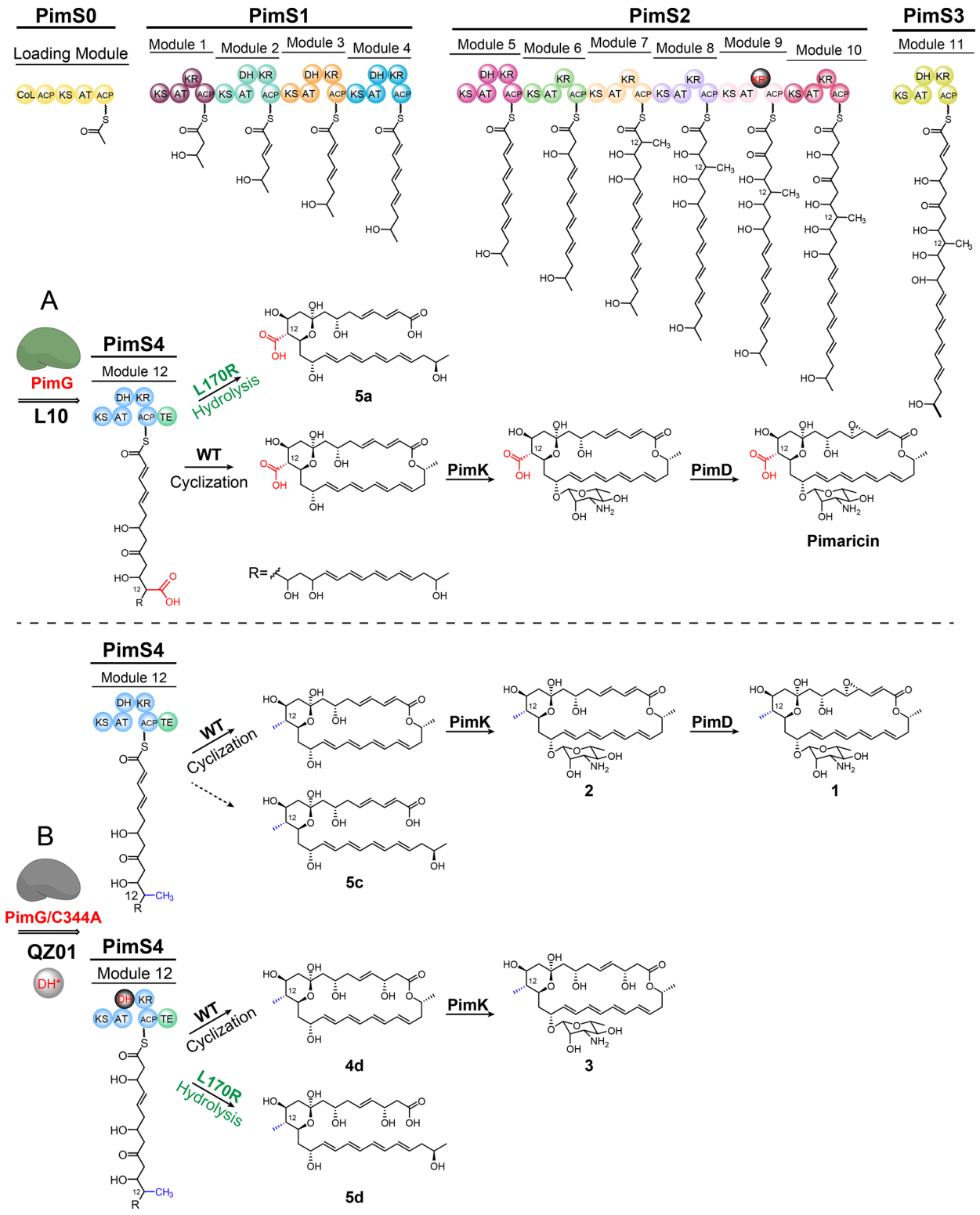

Figure 1. Proposed biosynthetic pathway of pimaricin and decarboxylated pimaricin derivatives. (A) Proposed natural biosynthetic pathway of pimaricin in the wild-type (WT) strain *Streptomyces chattanoogensis* L10. KS, ketosynthase; AT, acyltransferase; KR, ketoreductase; DH, dehydratase; and KR*, inactive KR. P450 monooxygenase PimG is active and catalyzes the oxidation of C12-CH_3 into C12-COOH. Compound **5a** was accumulated after TE^{L170R} mutation in *S. chattanoogensis* L10. **5a**, 4,5-desepoxy-12-carboxy pimaricin polyketide chain. (B) Biosynthetic pathway of decarboxylated pimaricin derivatives in the mutant strain QZ01. DH*, DH domain with partial activity. Strain QZ01: PimG inactivation via C344A site-directed mutagenesis in *S. chattanoogensis* L10. Compound **5c** is a putative linear polyketide intermediate in the biosynthesis of decarboxylated pimaricin derivatives. Compound **5d** is accumulated via TE^{L170R} mutation in QZ01. **1**, 12-decarboxy-12-methyl pimaricin; **2**, 4,5-desepoxy-12-decarboxy-12-methyl pimaricin; **3**, 2-hydro-3-hydroxy-4,5-desepoxy-12-decarboxy-12-methyl pimaricin; **4d**, 2-hydro-3-hydroxy-4,5-desepoxy-12-decarboxy-12-methyl pimaricin macrolactone; **5c**, 4,5-desepoxy-12-decarboxy-12-methyl pimaricin polyketide chain; and **5d**, 2-hydro-3-hydroxy-4,5-desepoxy-12-decarboxy-12-methyl pimaricin polyketide chain.

https://doi.org/10.1021/acscatal.1c04991
ACS Catal. 2022, 12, 762−776

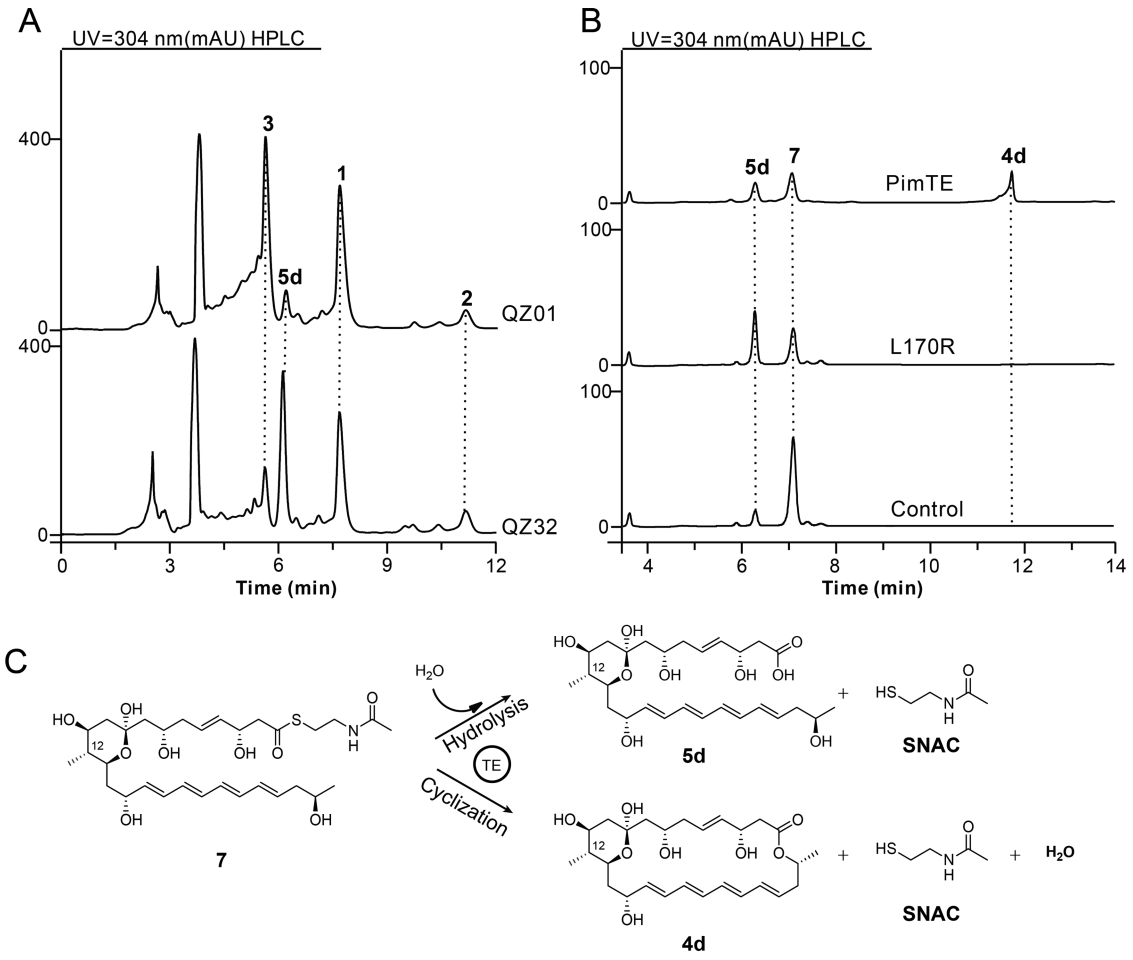

Figure 2. HPLC profiles of Pim TE_{L170R} mutations and *in vitro* enzymatic analysis of Pim TE. (A) Pim TE^{L170R} mutation in QZ01 resulted in accumulation of the full-length linear decarboxylated pimaricin intermediate **5d**. QZ01: PimG/C344A mutant strain; QZ32: QZ01 with Pim TE^{L170R} mutation. (B) HPLC profile of the *in vitro* enzymatic reaction of Pim TE using **7** as a substrate. Pim TE: the reaction of purified wild-type Pim TE with substrate **7**. L170R: the reaction of purified L170R mutated Pim TE with substrate **7**. Control: the reaction of PBS buffer with substrate **7**. (C) Reaction scheme of hydrolysis and cyclization catalyzed by Pim TE using compound **7** as a substrate analogue. **7**: Chemical derivation of the full-length linear pimaricin polyketide chain **5d** by *N*-acetylcysteamine (SNAC). **4d**: 26-membered macrolactone cyclized by Pim TE. **5d**: Hydrolyzed product released by Pim TE.

TE domains typically catalyze macrolactone formation in two steps, i.e., transesterification of a linear intermediate from ACP to a catalytic serine of TE and product offloading via intramolecular nucleophilic attack.[11] The first step is supposed to possess high substrate flexibility, while the macrolactone formation step is far more stringent. High-resolution crystal data of a few PKS TEs provide structure-based insights into the catalytic mechanism and substrate selectivity of TE-catalyzed PKS chain release. The macrocyclizing TEs from the erythromycin (DEBS TE)[8] and pikromycin (Pik TE)[12−14] biosynthetic pathways direct the formation of 12- or 14-membered macrolactones by hydrogen-bond contacts or hydrophilic barriers induced by structural restraints.[14−16] Moreover, the Pik TE domain was found to have limited substrate flexibility and functions as a gatekeeper in the processing of unnatural epimerized substrates. Site-directed engineering of Pik TE at the active site TE_{S148C} illustrated increased substrate flexibility and enabled the production of diastereomeric macrolactone *in vitro*.[17]

Polyene macrolides, including pimaricin, nystatin, amphotericin, and candicidin/FR-008, are structurally characterized by polyhydroxylated cyclic lactones comprising 20−40 carbons with three to eight conjugated double bonds (polyene moiety)[4] (Figure S1), which possess excellent antifungal activities and rare drug resistance. Polyene antibiotics are synthesized by type I modular PKSs and modified with one or two steps of oxidation[18,19] and glycosylation[20] (Figure 1). After elongation by multiple catalytic domains organized into a series of distinct modules, the TE domains cyclize and offload fully mature polyene intermediates. Polyene TEs are highly conserved but seem to be a unique group of PKS TE domains for specific lactonization of polyhydroxylated intermediates with continuous conjugated double bonds (Figures S1 and S2), which share relatively low sequence similarity with the canonical DEBS and Pik TEs from the erythromycin and pikromycin biosynthetic gene clusters. However, polyene antibiotics show relatively high toxicity to mammalian cells, which limits their application in clinical practice.[21−23] Recently, inactivation of the P450 monooxygenases AmphN,[24] RimG,[25] FscP,[26] or NysN[27] in corresponding polyene producers resulted in the accumulation of decarboxylated polyene derivatives with a methyl group instead of a carboxyl group (Figure S1). These derivatives display unexpected decreases in cell toxicity between 1−80 times

https://doi.org/10.1021/acscatal.1c04991
ACS Catal. 2022, 12, 762−776

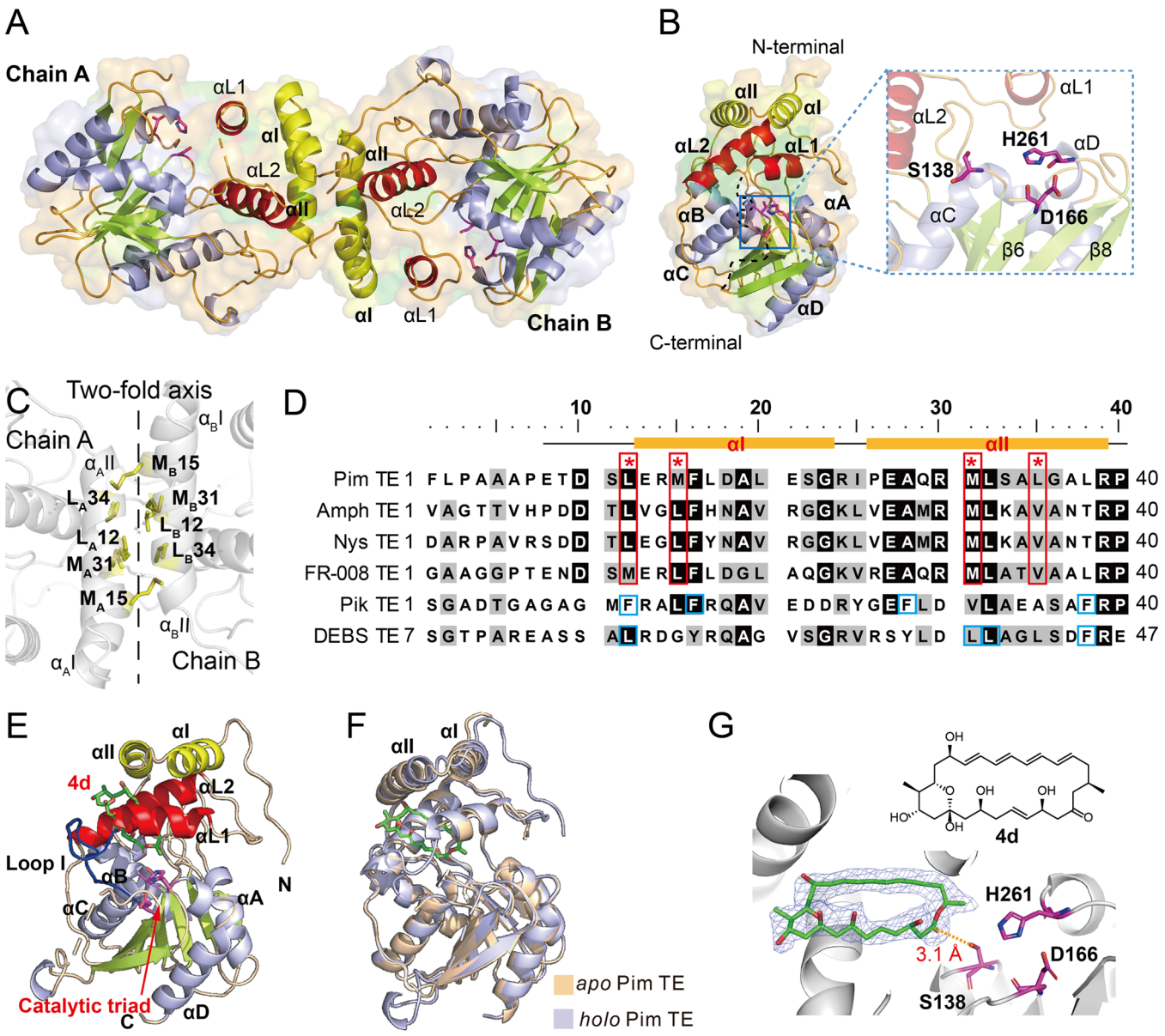

Figure 3. Overall structures of *apo*-Pim thioesterase (TE) and *holo*-Pim TE. (A) *apo*-Pim TE dimer structure. The α/β hydrolase core consists of α-helixes (light blue) and β-sheets (light green). The dimer-forming α-helixes αI and αII (yellow), α-helixes αL1 and αL2 involved in substrate channel formation (red), and flexible loop regions (light yellow) are indicated. The dimer interface of *apo*-Pim TE is 747.9 Å^2 calculated by PDBe (https://www.ebi.ac.uk/pdbe/pisa/). (B) Conserved catalytic triad S138-D166-H261 of *apo*-Pim TE (residues in purple). Electronic density of two loops (black dotted lines) is missing in *apo*-Pim TE. (C) Hydrophobic dimer interface of Pim TE consisted of two leucines (L12, L35) and two methionines (M15, M31). (D) Sequence alignment of amino acid residues involved in the formation of the PKS TE dimer interface. Four dimerization-critical residues in *apo*-Pim TE are highlighted by asterisks. The putative residues responsible for dimerization of polyene TE domains (red rectangles) and residues participating in the respective formation of DEBS TE and Pik TE (blue rectangles) are indicated. Pim TE, pimaricin TE domain; Amph TE, amphotericin TE domain; Nys TE, nystatin TE domain; Can/FR-008 TE, candicidin/FR-008 TE domain; Pik TE, pikromycin TE domain; and DEBS TE, erythromycin TE domain. The sequence accession numbers are listed in Table S3. The secondary structure is annotated based on *apo*-Pim TE. (E) Overall structure of *holo*-Pim TE. Cyclic product **4d** docked in the substrate channel is shown as green sticks. The loop I region (dark blue) is missing in *apo*-Pim TE. (F) Overlap structures of *apo*-Pim TE and *holo*-Pim TE. (G) Refined 2*Fo*-*Fc* map (dark blue) of cyclic product **4d** trapped in the substrate channel of *holo*-Pim TE. Catalytic triads (S138-D166-H261) are colored in purple. The distance between atom C1 of cyclic product **4d** and active site S138 is marked as the yellow dotted line.

while maintaining the antifungal activity[21] and are envisioned as new-generation substitutes of polyene antibiotics.[22] However, the titers of these unnatural decarboxylated polyene derivatives in AmphN-null and NysN-null strains were less than 2% of their parent antibiotic titers.[21] Similarly, three decarboxylated pimaricin derivatives (**1**, **2**, and **3**; Figures 1 and S1) were obtained by inactivating the P450 monooxygenase gene *pimG*/*scnG* in the pimaricin producer *Streptomyces chattanoogensis* L10.[28,29] The total amount of these derivatives (**1**, **2**, and **3**) in mutant QZ01 was up to 25% of the pimaricin titer in the wild-type strain.[28]

Considering that the titers of all of the decarboxylated polyene derivatives are reduced, we hypothesize that the low titer of these polyene derivatives is caused by inefficient recognition and processing of downstream enzymes toward the unnatural intermediates, especially the TE domain, which acts

https://doi.org/10.1021/acscatal.1c04991
ACS Catal. 2022, 12, 762−776

as a gatekeeper during the formation of polyketide backbones. In this work, the structure of the pimaricin TE (Pim TE) domain complexed with a 26-membered macrolactone was determined to provide mechanistic insight into the TE domain-catalyzed polyene lactonization. The TE bottlenecks in polyene biosynthesis were determined and engineered based on molecular dynamics (MD) simulations. *In vitro* enzymatic analysis using a full-length linear polyene intermediate as a substrate was performed to evaluate the activities of TE mutants generated by site-directed mutagenesis. Lastly, the TE mutations were also introduced *in vivo* to improve the titers of less toxic decarboxylated polyene derivatives. Our work may shed new light on the titer increase of unnatural polyketide derivatives via TE engineering.

RESULTS

Establishment of the Pim TE Catalysis System with a Fully Elongated Linear Polyketide Intermediate 5d. To improve the titer of decarboxylated pimaricin derivatives, homologous modeling based on Pik TE (PDB: 2H7X) was initially applied to guide the engineering of Pim TE, although the amino acid sequence identity between Pim TE and Pik TE was as low as 32.85%. Among the three Pim TE mutants (L170R, L213R, N214L) that did not contribute to the titer increase of decarboxylated pimaricin derivatives, the mutated Pim TE^{L170R} in *pimG*-deleted strain QZ01[28] substantially accumulated compound **5d** (m/z = 509.2756 ([M − H]$^-$)), which appeared as a minor component in QZ01 (Figures 2A and S4). Through LC-MS/MS and NMR spectroscopy analysis, compound **5d** was characterized as 2-hydro-3-hydroxy-4,5-desepoxy-12-decarboxy-12-methyl pimaricin ($C_{27}H_{42}O_9$) (see the Supporting Information) and considered to be a fully elongated linear decarboxylated pimaricin intermediate. The same TE^{L170R} mutation was also introduced into the wild-type strain *S. chattanoogensis* L10 (ZYC01, Figures S3 and S5) and accumulated another full-length linear polyketide **5a** (m/z = 521.2392 ([M − H]$^-$), Figure S5D), which was speculated to be the natural intermediate that tethered to the ACP12 domain during the biosynthesis of pimaricin (Figure 1A).

Using compound **5d** as a substrate, an *N*-acetylcysteamine (SNAC) derivative was subsequently synthesized (Figures S6 and S7) according to the method published by Hansen et al.[30] and named compound **7**. In the *in vitro* enzymatic assay, Pim TE catalyzed macrolactonization or hydrolysis of compound **7** to cyclic product **4d** or linear product **5d** (Figures 2B,C, S8, and S9). Since more than 50% of compound **7** was converted after 3 h incubation with 100 μM purified Pim TE, this system could be efficiently used to evaluate the catalytic activities of different Pim TE mutants (Figure 2B). For example, the mutated Pim TE^{L170R} showed reduced substrate conversion but accumulated more hydrolyzed linear product **5d** (Figure 2B), in accordance with the *in vivo* results (Figure 2A). In addition, compound **7** also served as a ligand for the cocrystallization of Pim TE.

Crystallization of the *apo*-Pim TE and *Holo* Structure of Pim TE Complexed with a 26-Membered Macrolide. To gain an accurate structural model for investigating potential bottlenecks during the chain release catalyzed by Pim TE toward the unnatural intermediate with C12-CH_3, we sought to elucidate the crystal structure of ligand-free Pim TE by X-ray diffraction. When coexpressed with the ACP12-TE linker, the soluble expression of Pim TE was significantly optimized (Figure S10). However, the subsequent crystallization of purified 305-aa Pim TE failed. Alternatively, a tobacco etching virus (TEV) protease digestion site was inserted between the ACP12-TE linker and the Pim TE domain, aiming to remove the linker from the 305-aa Pim TE after soluble expression and Ni affinity chromatography purification (Figure S10D,E). The 286-aa Pim TE was finally subjected to crystal screening and X-ray diffraction (Figure S10F). A 2.10 Å Pim TE structure was elucidated using molecular replacement with Pik TE (2H7X) as the search model (R_{work} = 20.42%, R_{free} = 25.03%; Table S3, PDB: 7VO4).

In the *apo*-Pim TE structure, two Pim TE molecules were present in a crystallographic asymmetric unit. Each monomer adopts a conserved α/β-hydrolase fold similar to other I PKS TEs, including two extra α-helices at the N-terminal (αI and αII; Figure 3A,B) and a lid region (loop I (loop L168-D179), αL1, loop II (loop M189-N200), αL2) between β6 and β7 (Figure S11). Notably, the proper conformation of the first two α-helices, αI/αII, is essential for Pim TE dimerization. The hydrophobic dimer interface (747.9 Å^2) is formed by a series of hydrophobic residues (L12, M15, M31, L35), which are conserved in polyene TEs as well as in DEBS TE and Pik TE (Figure 3C,D). However, the electronic density of the two loop regions (loop I and loop F235-S250) is missing in the *apo*-Pim TE (Figures 3B and S11).

Subsequently, linear compound **7** was incubated with Pim TE for cocrystallization. After data collection and molecular replacement using *apo*-Pim TE as the search model, a 2.40 Å *holo* structure of the Pim TE domain complexed with a 26-membered macrolactone (2-hydro-3-hydroxyl pimaricinolide, **4d**) was elucidated (Figure 3E and Table S3, PDB: 7VO5). Interestingly, the remaining catalytic activity of Pim TE resulted in the cyclic product **4d** embedded in Pim TE, rather than compound **7** or the linear hydrolyzed product **5d**. The conserved α/β hydrolase core was unchanged (RMSD = 0.331) in both the *apo*-Pim TE and the *holo* structure of Pim TE-**4d**, except for a slight tilt of αI and αII for dimerization (Figure 3F). With the binding of a ligand in the substrate channel, the conformation of the loop I region becomes clear, which is a crucial part of the substrate channel (Figure 3E) and missing in *apo*-Pim TE. The product **4d** is ∼3.1 Å away from the active site S138 (Figure 3G), and the H-bond interaction between S139 and the C1-carbonyl group and the water bridge between C7-OH and Gln174 play key roles in trapping the cyclic product **4d** (Figure S12).

Structural Adaptation of the Polyene TE Substrate Channel for Chain Release of Amphiphilic Substrates. As shown in the Pim TE-**4d** complex, Pim TE is specifically engaged with a channel shape as two funnels opposite each other (Figure 4A). The N-terminal funnel is formed by αA, αD, and loop II with a mouth diameter of 8.6 Å. The C-terminal funnel (10.6 Å) is the substrate-binding pocket in the *holo* Pim TE structure, which is formed by three α-helices (αII, αL1, αL2) and the loop I region. The catalytic triads S138-H261-D166 are located at the narrowest part of the channel formed by the two joint tunnels (3.5 Å, Figure 4A).

The electrostatic surface representation of Pim TE reveals that the lid region, including the hydrophobic residues from αL1 and αL2 and the hydrophilic residues of the loop I region, forms an amphiphilic environment suitable for binding of a large amphiphilic polyene intermediate (Figures 4B and S13). The C16-C23 polyene moiety of the **4d** product contacts the L183-M184-M206-M210 hydrophobic cleft formed by αL1

https://doi.org/10.1021/acscatal.1c04991
ACS Catal. 2022, 12, 762−776

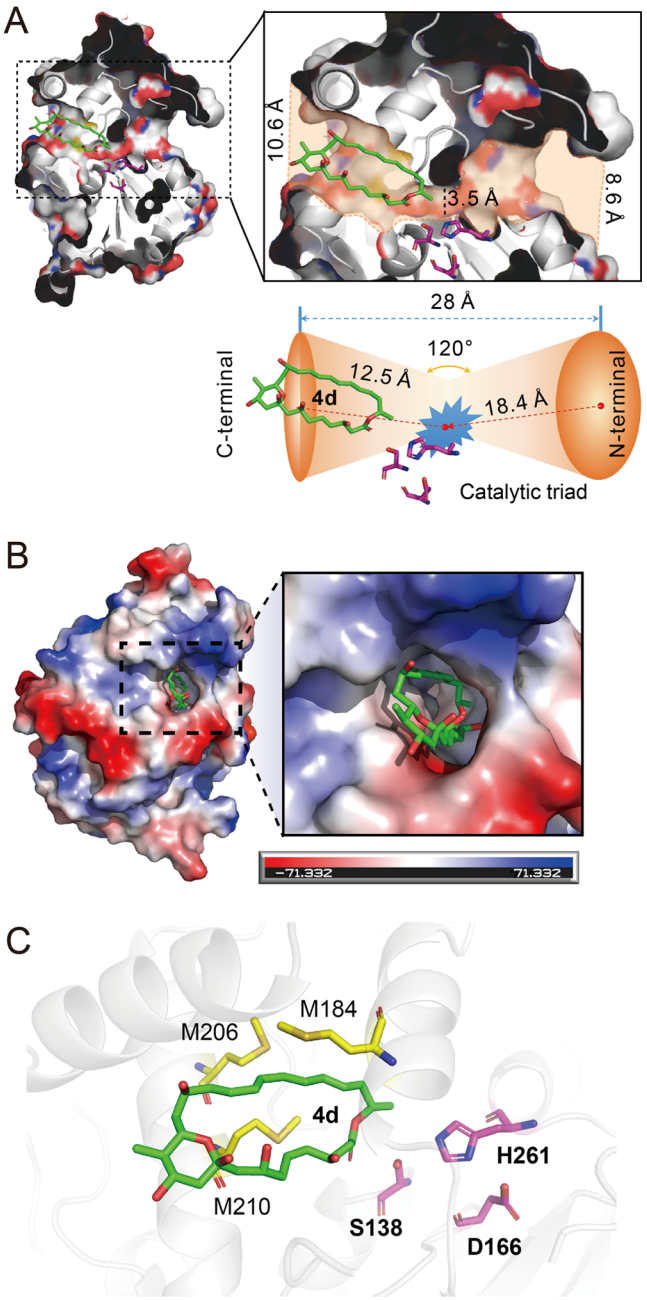

Figure 4. Structural insights into the Pim TE domain. (A) Cut-away view of the bifunnel-shaped channel in Pim TE. The cyclic product **4d** is shown as green sticks and the catalytic triad as purple sticks. (B) Electrostatic surface representation of the Pim TE substrate channel with the cyclic product **4d** (green sticks). The residues with a positive charge are colored in blue and those with a negative charge in red. (C) Hydrophobic residues involved in the formation of the hydrophobic cleft in *holo*-Pim TE. The related residues are highlighted by yellow sticks, the cyclic product **4d** is shown as green sticks, and the catalytic triad as purple sticks.

and αL2 to restrain the polyene moiety and push the distal C25-OH group to the active site (Figure 4C). Simultaneously, the hydrophilic loop I region binds the polyhydroxy moiety of the substrate to stabilize the reacting conformation.

Bottlenecks on Pim TE toward the Unnatural C12-CH_3 Intermediate with Mismatched Substrate Docking. Acylated enzyme models, including S138-covalent connections with both natural C12-COOH[28] and unnatural C12-CH_3 substrates (**5c**, $\Delta^{2,3}$-4,5-desepoxy-12-decarboxy-12-methyl pimaricin), were used for comparative studies of MD simulations (see Figures 1 and S14). These two covalent-binding complexes (Pim TE-**5a** and Pim TE-**5c**) were subjected to three times 100 ns MD simulations (Figures S15 and S16). Two distances were employed to evaluate the productive and unproductive conformations, including the Nε-O25 distance between the nucleophilic oxygen of C25-OH and the Nε nitrogen of H261 in the catalytic triad and the C1-O25 distance between the nucleophilic oxygen of C25-OH and C1 from the substrates. The former demonstrates deprotonation of the terminal hydroxyl group via H261, and the latter suggests the possibility of a subsequent nucleophilic attack on the substrates. Therefore, one simulation in the respective systems (Pim TE-**5a** and Pim TE-**5c**) with the most productive conformations close to the cyclized state defined by *d*(C1-O25) ≤5.0 Å and *d*(Nε-O25) ≤3.5 Å (i.e., conformation **I** in Figure S16) were further applied to perform additional 200 ns simulations (Figures S17 and S18) to investigate the details of the prereaction conformations.

The 300 ns simulations in the Pim TE-**5a** system demonstrate that substrate **5a** repeatedly adopts macrolactonization-favorable reacting conformations (**aI**, **aII**) in the first 250 ns (Figure S17). The conformation **aII** formed first and remained prevalent (43.0%; Figure S18A) at the beginning, where the distal hydroxyl group C25-OH was emplaced proximal to C1 (C1-O25 ≤5.0 Å) for macrolactonization. Once the C25-OH contacts the active site H261 (Nε-O25 ≤3.5 Å), subsequent deprotonation of C25-OH is promoted by H261, and the favorable conformation **aI** forms (Figure S18A). During 300 ns simulations, conformations **aI** and **aII** indicate high structural adaptability (59.6% in total) of Pim TE toward **5a** with C12-COOH. On the contrary, the unproductive conformation **cIV** in Pim TE-**5c** accounted for the majority (79.4% capacity) of the sampled conformers (Figure S18B,D), whereas the macrolactonization-favorable conformations **cI** and **cII** with an accessible distance of C1-O25 <5.0 Å hardly formed (Figure S17).

To further identify the molecular basis of the catalytic bottleneck of Pim TE toward the unnatural C12-CH_3 substrate, the H-bonding and hydrophobic interactions between Pim TE and substrates **5a** or **5c** were counted (Figure 5A). The H-bonding interactions near the C12 elbow were analyzed first. Substrate **5a** was observed to be not only H-bonded with Q29, M210, and N214 from αII and αL2 but also with a series of hydrophilic residues (D179, N175, H172, etc.) in the loop I region on the opposite side of the channel (Figure 5B). Specifically, the C12-COOH carboxylate group in substrate **5a** exhibited H-bonding interactions with Q29, Q174, N175, G211, and N214 (Figure 5C), which balances the hydrophilic network on both sides of the substrate channel. In contrast, the H-bonding interactions between the unnatural substrate **5c** and Pim TE decreased; in addition to an intensive hydrophilic interaction with Asp179 in the loop I region, substrate **5c** forms a weak interaction with N214 in αL2 (Figure 5D). Moreover, in the MD simulation of Pim TE-**5a**, the hydrophobic cleft that consists of I25, G182, L183, M210, and F262 is well aligned with the C16-C23 polyene moiety (Figure S19A), facilitating the stable and repeated emergence of the macrolactonization-favorable conformation of substrate **5a**. However, because of the lack of C12-COOH anchorage, the polyene-specific hydrophobic interaction was mismatched

https://doi.org/10.1021/acscatal.1c04991
ACS Catal. 2022, 12, 762−776

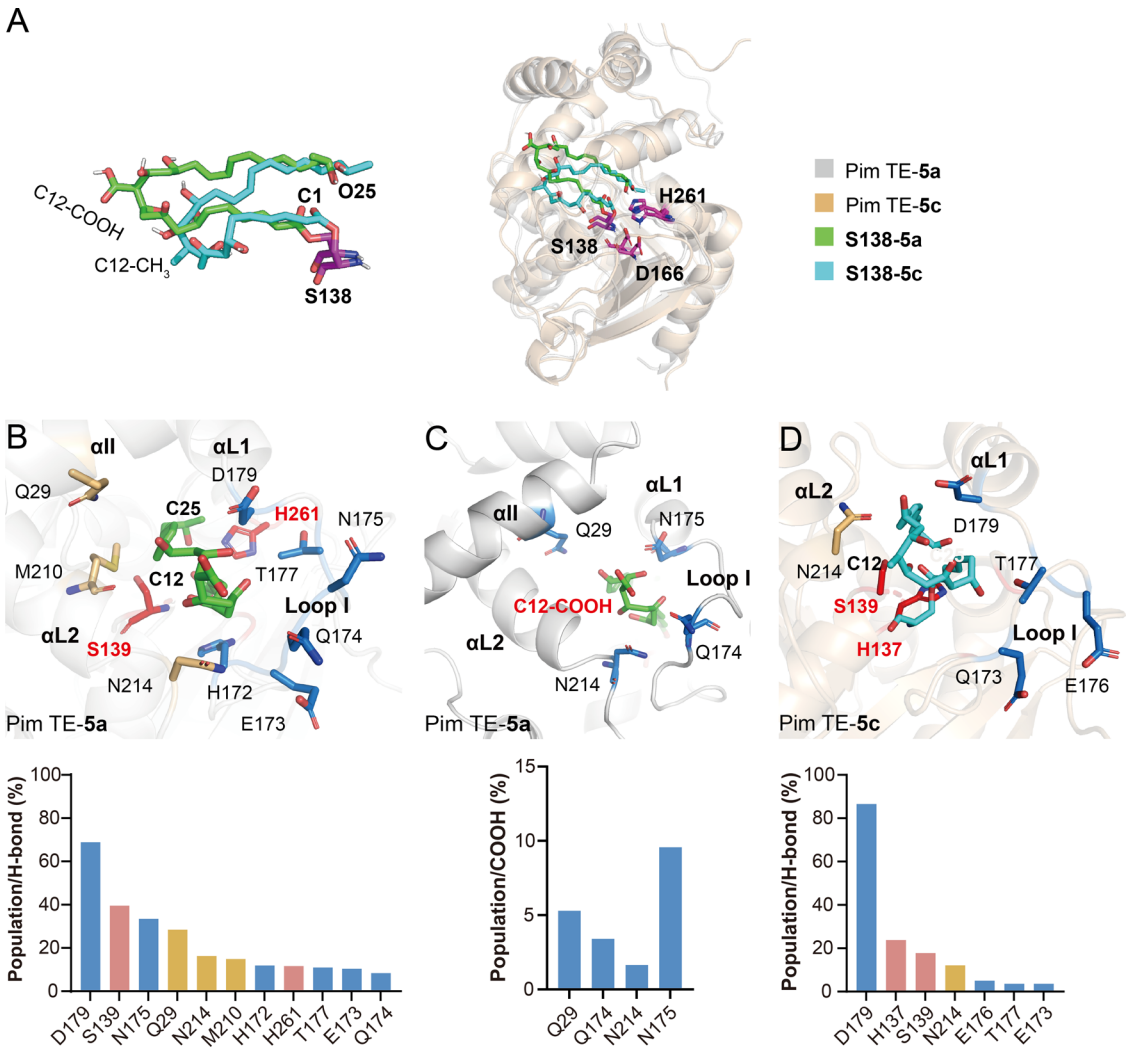

Figure 5. H-bonding interactions of Pim TE-catalyzed pimaricin chain release based on MD simulation. (A) Comparison of prereaction conformation of Pim TE-**5a** and Pim TE-**5c**. Unnatural substrate **5c** is twisted in the substrate channel when cyclized by Pim TE. Substrate **5a** is shown in green and substrate **5c** in blue. (B) H-bond interactions between Pim TE and substrate **5a**. The residues are colored as follows: from the loop I region (blue), from αII and αL2 (gold), and near active sites (red). (C) Key H-bond interactions between C12-COOH and Pim TE in MD simulation of Pim TE-**5a**. The related residues are highlighted in blue. (D) H-bond interactions between Pim TE and substrate **5c**. The residues are colored as follows: from the loop I region (blue), from αII and αL2 (gold), and near active sites (red).

and attenuated in the MD simulation of Pim TE-**5c** (Figure S19D).

Enhanced Release of Unnatural C12-CH_3 Pimaricin Derivatives via Structure-Directed Engineering of the TE Domain. Based on the addressed catalytic bottlenecks on the Pim TE-catalyzed chain release of polyene intermediates by crystal study and computational simulation, we performed site-directed mutagenesis of TE to enhance the release of the less toxic unnatural pimaricin derivatives (Figure 6). TE engineering was performed as follows: (1) introducing more feasible H-bond donors from αII and αL2 to balance the hydrophilic interaction between the unnatural substrate and Pim TE at the C12 elbow (Figure 6A); (2) enhancing the hydrophobic interaction between the substrate channel and C16-C23 conjugated double bonds to stabilize the distal hydroxyl group near the active site (Figure 6B); and (3) replacing hydrophobic residues in the active center with hydrophilic ones (Figure 6C). Seven residues (Q29, G182, R186, A207, M210, and G211) were selected and subjected to site-directed mutagenesis by PCR. *In vitro* activity analysis using compound **7** as a substrate enabled the identification of positive mutations with improved substrate conversion, which were subsequently applied to Pim TE engineering by homologous recombination in strain QZ01, producing C12-CH_3 pimaricin derivatives, including **1**, **2**, **3**, and **5d** (Figures S20 and S21).

First, Q29, A207, and G211 were selected to introduce more H-bond donors in αII and αL2 by Q29E, Q29D, Q29R, A207Q, G211H, or G211N mutations *in vitro*. Substitutions of Q29D, A207Q, G211H, and G211N showed significantly improved substrate conversions of 15.5, 39.2, 13.8, and 10.3%, respectively (Figure 6A, Supporting Data 1). Subsequently, TE^{Q29D}, TE^{A207Q}, and TE^{G211H} mutant strains were constructed. As expected, TE^{A207Q} and TE^{G211H} resulted in a 17.1 and 34.6% increase in the C12-CH_3 pimaricin derivatives, respectively, in comparison with that of QZ01 (Figure 6A and S22, Supporting Data 2). Second, to enhance the hydrophobic interaction between the Pim TE substrate pocket and the polyene moiety, G182 and M210 inside the hydrophobic cleft were mutated into G182A, G182V, M210F, and M210L *in vitro*. The G182A and M210L mutations with 5.0 and 33.2%

https://doi.org/10.1021/acscatal.1c04991
ACS Catal. 2022, 12, 762−776

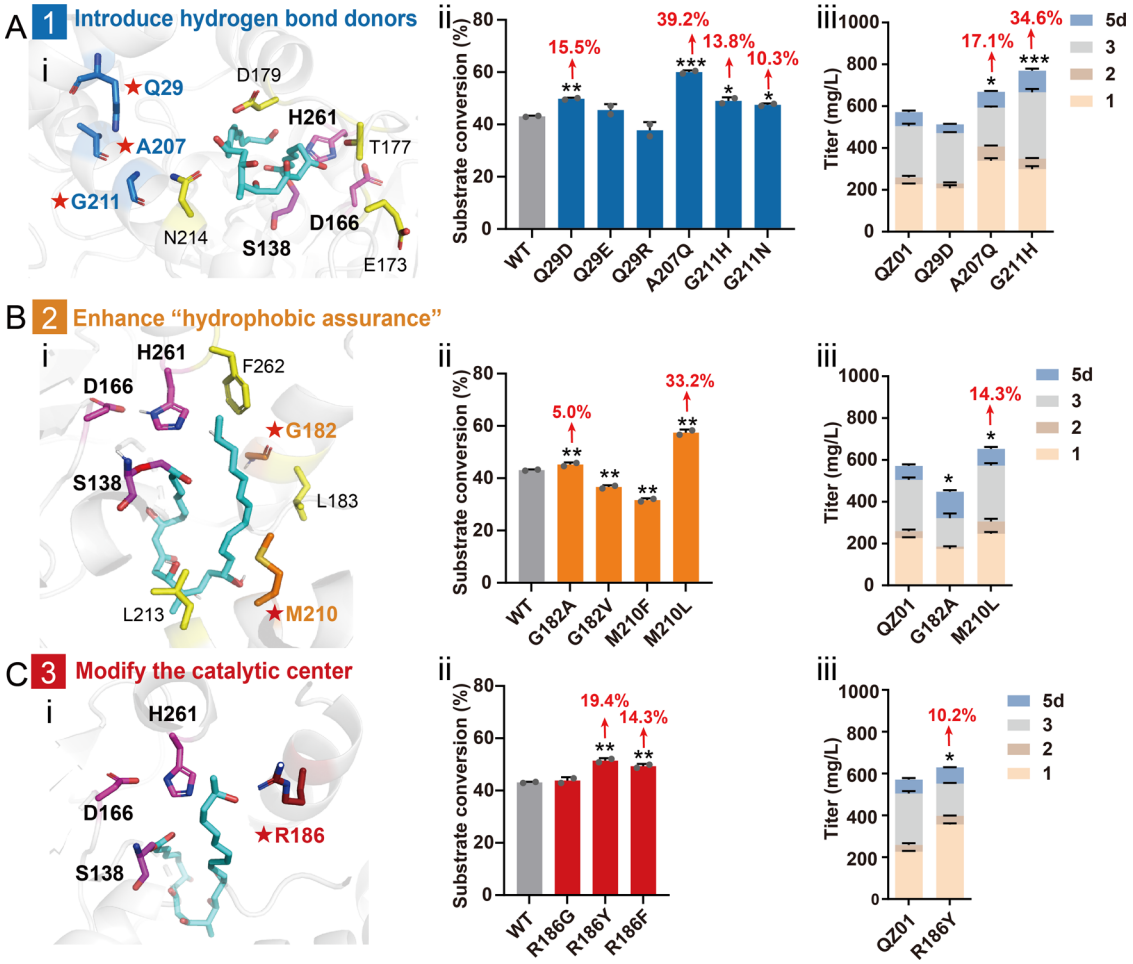

Figure 6. Structure-directed engineering of Pim TE. (A) Pim TE engineering by strategy 1. Pane i: the selected mutation targets Q29, A207, and G211 are highlighted as blue sticks; pane ii: substrate conversion of TE mutations Q29D, Q29E, Q29R, A207Q, G211H, and G211N evaluated by *in vitro* enzymatic analysis using analogue **7** as a substrate. Graphs depict means ± SD (n = 2 biological replicates). Statistical analysis was performed by the one-way ANOVA test. *p < 0.05, **p < 0.01, and ***p < 0.001. Source data and detailed p-values are listed in Supporting Data 1. Pane iii: the total titers of C12-CH_3 pimaricin derivatives **1**, **2**, **3**, and **5d** in TE^{Q29D}, TE^{A207Q}, and TE^{G211H}. Graphs depict means ± SD (n = 3 biological replicates). Statistical analysis was performed by the one-way ANOVA test. Source data and detailed p-values are listed in Supporting Data 2. (B) Pim TE engineering by strategy 2. Pane i: the selected mutation targets G182 and M210 are highlighted as orange sticks; pane ii: substrate conversion of TE mutations G182A, G182V, M210F, and M210L evaluated by *in vitro* enzymatic analysis. Pane iii: the total titers of C12-CH_3 pimaricin derivatives in TE^{G182A} and TE^{M210L}. (C) Pim TE engineering by strategy 3. Pane i: target site R186 highlighted by red sticks; pane ii: substrate conversion of TE mutations R186G, R186F, and R186Y evaluated by *in vitro* enzymatic analysis; pane iii: the total titers of C12-CH_3 pimaricin derivatives in TE^{R186Y}.

increased substrate conversion *in vitro*, respectively (Figure 6B, Supporting Data 1), were introduced into Pim TE in QZ01, and the accumulation of the C12-CH_3 pimaricin derivatives was increased by 14.3% in the mutant strain TE^{M210L} (Figure 6B and S23, Supporting Data 2). Third, the hydrophilic residue R186 was found to be competitively H-bonded to the distal hydroxyl group C25-OH (Figures S24 and S25). It was then mutated into the hydrophobic residues R186G, R186F, and R186Y *in vitro*. Substrate conversion of mutations R186F and R186Y increased by 14.3 and 19.4%, respectively (Figure 6C, Supporting Data 1). Notably, the modification of TE^{R186Y} *in vivo* near the Pim TE active center increased the total titers of C12-CH_3 pimaricin derivatives by 10.2%, among which the production of compound **1** was substantially increased by 57.4% (Figure 6C and S26, Supporting Data 2). The Pim TE was subsequently engineered by a combination of effective single mutations, and the total titers of C12-CH_3 pimaricin derivatives from the combined mutations of $TE^{A207Q/M210L}$ were increased by 37.1% at most among all of the mutants (Figure S27).

DISCUSSION

Manipulation of polyketide synthases and the related modification enzymes is an excellent strategy to generate an abundant pool of novel natural product analogues with modified structures and potent activities. However, the efficient accumulation of desired natural product analogues remains challenging. Recent work on Pik TE uncovered the TE bottleneck in polyketide processing, highlighting the important gatekeeper role of the TE domain in selecting and releasing unnatural substrates.[30,31] In this study, the fully elongated linear pimaricin polyketide intermediates **5a** and **5d** were obtained by introducing a site-specific mutation of L170R into the Pim TE domain. The full-length polyketide chain **5d** accumulated with a considerable titer of 234.4 mg/L (Figure 2A), accompanied by the accumulation of cyclized products **1**

https://doi.org/10.1021/acscatal.1c04991
ACS Catal. 2022, 12, 762−776

(161.6 mg/L) and **3** (59.3 mg/L). To date, few characterized examples of both macrocycles and free acids generated with considerable titers *in vivo* from the same native pathway have been reported.[11,32] Thus, it could be a beneficial strategy to release linear intermediates during PKS assembly by mutated TE domains, which will facilitate enzymatic characterization of both individual domains and modification enzymes of PKS biosynthetic machineries.

Nonetheless, the hydrolyzed linear intermediate **5d** further contributed to determining the first TE structure Pim TE from polyene PKSs complexed with a 26-membered cyclic product. The *holo* Pim TE structure revealed a unique bifunnel-shaped amphoteric substrate channel for the specific chain release of polyene polyketide intermediate with three to eight conjugated double bonds and polyhydroxy regions. As the most well-studied PKS TE domain, DEBS TE possesses a more polar active site chamber for the cyclization of a relatively hydrophilic macrolide, 6-deoxyerythronolide, by multiple H-bonded contacts.[8] The weak hydrophilic interactions between DEBS TE and substrates give DEBS TE relatively high substrate flexibility.[6] On the contrary, the polar channel in Pik TE induces the relatively hydrophobic 10-deoxymethynolide (10-DML) and narbonolide cyclized products to form a macrolide by the hydrophilic barrier.[14] The conjugated double bond system in 10-DML and narbonolide provides substrate conformational restraints for assisting cyclization by positioning the attacking hydroxyl group for macrolactone formation.[14] Herein, in polyene Pim TE, a spacious bifunnel-shaped channel is considered to be a characteristic conformation that induces the formation of large-sized polyene macrolides. Meanwhile, the H-bonding interactions, formed by the hydrophilic loop I region and hydrophilic residues from αII and αL2 with multiple hydroxyl groups in polyene intermediates, together with the hydrophobic interaction between the polyene moiety and hydrophobic cleft, guaranteed the efficient chain release of an amphiphilic intermediate. The homologous modeled structures of TE domains from amphotericin, nystatin, and candicidin/FR-008 biosynthetic pathways revealed that the amphiphilic distribution of residues in the lid region is conserved among polyene TEs for chain release of amphoteric polyene macrolides (Figures S28 and S29). In contrast, the lid regions from DEBS TE and Pik TE were more hydrophilic (Figures S28 and S29).

Among PKS TEs, the most diverse part of the enzyme structure is the αL1 and loop I region in the substrate channel. The length of the loop I region and the size of the final product were probably correlated. To date, the loop I region from Pim TE is the longest among all published PKS TE structures. TE domains with shorter loop I regions (a longer αL1, Figures S11 and S30), like DEBS TE and Pik TE, seem to release a short polyketide intermediate as a small-size macrolactone (12 membered 10-DML, e.g., 4.7 × 5.8 Å^2). However, for chain release of 26-membered (pimaricinolide, 12.7 × 5.1 Å^2) or even 38-membered polyene intermediates (amphotericinolide, 21.3 × 4.6 Å^2), a longer loop I is needed to provide a spacious pocket for accommodating large-size substrates (Figure S30). Notably, tautomycetin (TMC) TE that only catalyzes hydrolysis of polyketide intermediates in the biosynthesis of tautomycin possesses an even longer αL1 helix in the lid region, which forms a long and narrow substrate channel solely to release a linear product.[33] Therefore, editing the length and amino acid composition of the loop I region might help to expand the substrate tolerance on product size and form (cyclic or linear). However, to improve the cyclization of an unnatural substrate with the same ring size, the *in vitro* engineering of Pim TE within the loop I region, such as L170R, H172L, T177G, and D179R (Supporting Data 1), failed to increase the substrate conversion. Inappropriate mutations in the loop I region might cause reduced activities (especially macrolactonization) and accumulation of the hydrolyzed linear shunt-product **5d**, e.g., in Pim TE^{L170R} *in vivo*.

For thioesterase-catalyzed macrolactonization, valid conformation of the distal hydroxyl group at a nucleophilic attack-accessible distance to the proximal histidine and C1-carbonyl group is essential.[16,17] The MD simulation of Pim TE-**5a** and Pim TE-**5c** based on the accurate *holo* Pim TE structure indicated a higher proportion of macrolactonization-favorable conformation of the natural substrate with C12-COOH. The distal C25-OH of substrate **5a** is steadily placed proximal to the C1-carbonyl by H-bonding with S139 (Figure 6A), which is beneficial for conformation **aII** (43.0% capacity) formation. Accordingly, the proportion of deprotonation-critical H-bonding interactions between the Nε atom of H261 and the distal hydroxyl group C25-OH was almost five times higher in Pim TE-**5a** than in Pim TE-**5c** (Figure S24). Moreover, H-bond interactions at the C12 elbow were deduced to provide an anchor for bending the linear intermediate into a pre-macrolactonization conformation, subsequently facilitating the deprotonation of C25-OH by H261 to obtain the tetrahedral intermediate by intramolecular nuclear attack. The nonpolar C12-CH_3 group, instead of the polar carboxyl group, in unnatural substrate **5c** could result in unbalanced H-bonding interactions at the C12 elbow and curled substrate **5c** docking in Pim TE. Thus, the terminal hydroxyl C25-OH of **5c** is proximal to the hydrophilic residues near the active center (Figure S25), which disturbs the deprotonation of C25-OH by H261 to form a macrocyclized product. Briefly, the TE bottlenecks on the Pim TE-catalyzed chain released an unnatural substrate with the C12-CH_3 cloud can be summarized as follows: (1) holding the appropriate and stable pose for the distal C25-OH from substrate **5c** to the active site in a macrolactonization-suitable conformation is difficult because of the lack of accessible H-bond donor residues in αII and αL2 to balance the hydrophilic network at the C12 elbow; (2) the hydrophobic interaction between the polyene moiety and hydrophobic cleft was attenuated upon the macrocyclization of unnatural substrates with C12-CH_3; and (3) the distal C25-OH is easily trapped by competitive hydrophilic residues near other active sites rather than at the H261 site to form a macrolactonization-favorable conformation.

Growing evidence suggests that the TE domain could be an important target for PKS engineering to substantially accumulate unnatural polyketide analogues. In the full-module processing of unnatural pentaketides, the engineering of the Pik TE active site S148C displays gain-of-function processing of substrates with inverted hydroxyl groups.[17] The S148C in Pik TE provides a mechanistic change during the macrolactonization step from a two-step transesterification in the original TE reaction to a lower-energy single-concerted step in the Pik TE$_{S148C}$ pathway.[30] In addition, domain swapping of TMC TE with Pik TE in the biosynthesis of the linear polyketide tautomycin resulted in the accumulation of the trace macrocyclic product.[32,33] Both studies on TE engineering demonstrated the fascinating capacity of the modified TE

https://doi.org/10.1021/acscatal.1c04991
ACS Catal. 2022, 12, 762−776

domain toward unnatural substrates.[32,33] Pim TE engineering was also employed to increase the titers of C12-CH_3 pimaricin derivatives. Notably, the *in vitro* enzymatic analysis system based on the full-length linear polyketide intermediate **5d** further accelerated the screening of positive TE mutations. Although only one to three mutation(s) for each target site were subjected to *in vitro* enzymatic analysis, at least one effective mutation with increased substrate conversion was obtained. Based on the interactive and precise design of the TE domain, four single mutations in seven target sites showed increased chain release of C12-CH_3 pimaricin derivatives *in vivo*. The A207Q and G211H mutations in αL2 were first selected to provide available H-bond donors to interact with hydroxyl groups near the C12 elbow, contributing to the recovery of the balanced H-bonding network. The cyclic pimaricin derivatives produced by Pim TE^{G211H} were improved at most by 34.6% among all mutants (Supporting Data 2). In fact, the effective mutation R186Y might not only weaken the undesired hydrophilic interaction with C25-OH but also hold $\pi-\pi$ stacking interactions with Phe262, which stabilizes the active residue H261 indirectly.

In engineered PKS systems, the production of unnatural products usually decreases or fails entirely.[6,31] The biochemical mechanism underlying this remains elusive. This work provides another example of a TE bottleneck when processing an unnatural intermediate with modified structures. This is the first report on TE engineering with increased titers of unnatural polyketide analogs guided by protein structural elucidation and computational simulation. Nonetheless, the SNAC derivation of natural intermediate **5a** and the macrolactonization or hydrolysis of the substrate analogue with a C12-carboxyl group by Pim TE *in vitro* remain inaccessible. The cocrystal structure of Pim TE complexed with natural intermediate **5a** or the cyclic product with C12-COOH may straightforwardly provide deeper insights into the polyene TE-catalyzed chain release. Moreover, proper starting points and mutation targets play key roles in obtaining the desired improvements during protein engineering.[34] In the future, further specific titer improvements of C12-CH_3 pimaricin derivatives, especially cyclized product **1** and **2**, with substantially reduced toxicity will be conducted according to MD simulation and the structures of mutated Pim TEs. Furthermore, as low titers of less toxic decarboxylated derivatives occurs in all clinically important polyene antibiotics,[4,21,24] such as amphotericin and nystatin, precise TE engineering for other polyene producers should be performed.

CONCLUSIONS

Inspired by the distinct decrease in the titers of decarboxylated polyene antibiotics and the potent TE bottleneck in polyketide processing, this work focused on investigating the unique catalytic mechanism of polyene TEs in the formation of 20−40 membered amphiphilic macrolides. Through incubation with an activated full-length linear polyketide intermediate, a 26-membered macrolide-complexed polyene TE domain structure was determined, providing a mechanistic insight into the Pim TE-catalyzed chain release of amphiphilic intermediates. An amphoteric bifunnel-shaped substrate channel was identified to be providing a hydrophobic cleft for docking continuous conjugated double bonds and a H-bonding network, woven by hydrophilic residues from the αL2, αII, and loop I regions, to organize the pre-macrolactonization conformation of the linear substrate. The key C12-COOH plays a critical role in stabilizing the macrolactonization-favorable conformation of the natural substrate by balancing the H-bond interaction at the C12 elbow. Thus, the distal C25-OH of the natural substrate is steadily restrained at a deprotonation-accessible distance by H-bonding interactions with S139, promoting the efficient chain release by Pim TE. In addition, bottlenecks in processing the unnatural intermediate with C12-CH_3 were overcome through TE mutations, as guided by protein structure analysis and MD simulations. Aided by the rapid *in vitro* enzymatic screening of mutated TEs, the titers of the less toxic pimaricin derivatives with C12-CH_3 were significantly increased through TE mutations *in vivo*. Therefore, the PKS TE domain was interactively designed in this work according to protein−substrate interactions, which shed new light on how the titers of novel but unnatural polyketide derivatives with promising activities could be improved.

EXPERIMENTAL METHODS

Bacterial Strains, Plasmids, and Culture Conditions. The strains, plasmids, and primers used in this study are listed in Tables S1 and S2. DNA isolation and manipulation were performed according to the standard protocols. Primer synthesis and DNA sequencing were performed by Sangon Biotech (Shanghai, China). *Streptomyces chattanoogensis* L10 (CGMCC 2644) and the mutants were cultured on ISP2 agar plates for sporulation at 30 °C for 7−9 days. The ISP2 agar plate consisted of a yeast extract (4 g/L), malt extract (10 g/L), glucose (4 g/L), pH 7.4−7.5, and agar (19.2 g/L), autoclaved at 115 °C for 20 min. The ISP2 agar plates were used for conjugation between *Escherichia coli* and the *Streptomyces* strains. For the fermentation of pimaricin and its derivatives, *S. chattanoogensis* L10, QZ01, and the related mutant strains were cultured on a YSG medium (glucose (60 g/L), soybean meal (28 g/L), and yeast extract (7 g/L) at pH 7.2). *Escherichia coli* DH10B was used for plasmid construction. *E. coli* BL21(DE3) was used for heterologous overexpression of Pim TE proteins and the mutated proteins. *E. coli* ET12567(pUZ8002) was used for conjugation to deliver plasmids into *Streptomyces* strains. All *E. coli* strains were grown at 37 °C in LB broth and LB agar.

Fermentation and HPLC Analysis of Pimaricin Derivatives. The fermentation of the QZ01 and Pim TE mutants was performed as previously described.[28] The titers of pimaricin derivatives were evaluated by HPLC analysis (1260 Infinity II LC System; Agilent, Santa Clara, CA) with a TC-C18 column (4.6 × 250 mm^2, particle size 5 μm; Agilent) using a mobile phase containing 67% Milli-Q water with 0.1% formic acid (A) and 33% acetonitrile (B) at a flow rate of 1 mL/min (10 min per sample). The signal detected at 303 nm was calculated according to the corresponding standard curve of pimaricin using Excel and GraphPad Prism 8.

Purification and Structural Elucidation of the Full-Length Linear Pimaricin Intermediate 5d. Overall, 5 L of fermentation broth of strain QZ32 was collected after being cultivated in a YSG medium at 30 °C for 5 days. The crude extract of compound **5d** was generated by extracting the collected sediment by methanol three times and then separated and fractionated by reversed-phase chromatography (250 × 25 mm^2, particle size 50 μm; YMC, Kyoto, Japan) eluted with a gradient of 10, 30, and 100% methanol. Compound **5d** was enriched in the fractions containing 30% methanol. The collected fraction was further purified by HPLC (33% acetonitrile, flow rate: 3 mL/min, UV: 303 nm) with a

https://doi.org/10.1021/acscatal.1c04991
ACS Catal. 2022, 12, 762−776

Thermo BDS HYPERSIL C18 column (250 × 10 mm^2, particle size 5 μm). To determine the chemical structures of these compounds, 1D- and 2D-NMR and high-resolution electrospray ionization mass spectroscopy (HR-ESI-MS) experiments were performed.

Preparation of Substrate Analogue 7. Compound **5d** (20.4 mg, 0.04 mmol, 1.0 equiv) and EDC·HCl (25.3 mg, 0.12 mmol, 3.0 equiv; Sigma, St. Louis, MO) were mixed in a 50 mL round bottom flask, and the flask was cooled to 0 °C. DMSO (10 mL, 10% v/v) was added, and the resulting solution was stirred at 0 °C for 30 min. Then, HSNAC (33.4 mg, 0.28 mmol, 7.0 equiv; Sigma) was added and stirred at 0 °C for an additional 10 min followed by DMAP addition (1.22 mg, 0.01 mmol, 0.25 equiv; Sigma). The solution was stirred at 0 °C for 10 min and transferred to a shaker (120 rpm) at 23 °C for 16 h. The reaction product was separated by reversed-phase chromatography, eluted with 100% methanol, and fractions containing the target product **7** were further subjected to preparative HPLC.

LC-Q-TOF-MS and LC-Q-TOF-MS/MS Analysis of Compounds 5a, 5d, and 7. The new compounds **5a**, **5d**, and **7** were first analyzed by qualitative tandem liquid chromatography quadrupole time of flight mass spectrometry (LC-Q-TOF-MS) and further confirmed by LC-Q-TOF-MS/MS. An Agilent 6545 Q-TOF mass spectrometer (Agilent) was used with an Agilent 1290 Infinity II HPLC system coupled with an electrospray ionization (ESI) source. A TC-C18(2) column (I.D. 5 μm, 4.6 × 250 mm^2; Agilent) was employed for chromatographic separation at 30 °C. The mobile phase consisted of a 67% solvent A (0.1% formic acid in distilled water) and a 33% solvent B (acetonitrile). The flow rate was set to 0.4 mL/min. The ESI probe apparatus was operated in a negative mode. All data were collected and analyzed using Mass Hunter software (Agilent).

***In Vitro* Enzymatic Analysis of Pim TE.** The enzymatic reaction of Pim TE was carried out in 50 mM PBS buffer (pH 8.0) with 100 μM purified Pim TE protein or its mutant proteins and 10 μM substrate analogue **7** at 30 °C for 3 h. Then, the reaction was terminated by adding two volumes of methanol centrifuged at 15 777*g* for 2 min. The supernatant was analyzed by HPLC (Agilent 1260 Infinity II LC System). The HPLC was operated at a flow rate of 1 mL/min with a TC-C18 column (250 × 4.6 mm^2, particle size of 5 μm) and detected at 303 nm. The mobile phase contained a 0.1% formic acid solution (A) and acetonitrile (B) with the following gradient: 0−8 min, 33% B; 8−13 min, 75% B; 13−15 min, 75% B; 15−18 min, 33% B; and 18−20 min, 33% B.

Cloning, Expression, and Purification of Pim TE. The Pim TE domain was first cloned and expressed, resulting in a final product consisting of 286-aa residues (Figure S10A). Detailed DNA sequences and related amino acid sequences are provided in the Supporting Information. The 286 Pim TE was amplified using the primers 286TE-F/R by PCR. After sequencing, 286 Pim TE was ligated into *Nde*I/*Hin*dIII-digested pET28a to generate pLQ951 (Figure S10B). The recombinant plasmid was transformed into *E. coli* BL21(DE3) cells for protein expression. Individual colonies were picked and cultivated in LB broth containing 50 μg/mL kanamycin at 37 °C until the OD_{600} reached 0.4−0.6. The cells were then induced with 0.3 mM IPTG for 20 h at 16 °C and harvested by centrifugation. The binding buffer with 500 mM NaCl and 50 mM Tris−HCl (pH 7.5) was used to resuspend cells for cell lysis by ultrasonication. To confirm the expression of His-tagged Pim TE protein, samples of induced cells, cell lysis supernatant, and cellular debris were analyzed by 12% sodium dodecyl sulfate-polyacrylamide gel electrophoresis (SDS-PAGE). After centrifugation at 15 777*g* for 40 min, proteins from the soluble fraction were purified using Ni-Sepharose 6 Fast Flow (GE Healthcare, Chicago, IL) at 4 °C. The His-Pim TEs were washed with 50 mL of binding buffer containing 15 mM imidazole and 10 mL of binding buffer with 50 mM imidazole, and then eluted with 5 mL of binding buffer containing 250 mM imidazole. NTA-purified proteins were further purified by FPLC (Bio-Rad, Hercules, CA) with a Superdex 200 gel filtration column (GE Healthcare) using buffer containing 150 mM NaCl and 10 mM Tris−HCl (pH 7.5). Finally, the proteins were concentrated and ultrafiltered to 13.5 mg/mL and subjected to crystallization.

305Pim TE with an 18-aa ACP-TE-linker inserted at the N-terminus was amplified using the primers 305TE-F/286TE-R (Figure S10A). The 305Pim TE was cloned into pET28a by *Nde*I/*Hin*dIII and generated pLQ952, which showed much better soluble expression in *E. coli* (Figure S10C). pLQ953 was designed to remove the 18-aa ACP-TE-linker by TEV protease after soluble expression and purification (Figure S10A,D). pLQ953 was divided into four parts, amplified by the primers 28a-1F/R, 28a-2F/R, 28a-3F/Lk-286TE-3R, and Lk-286TE-4F/28a-4R, respectively, and ligated using a Gibson assembly. The TEV protease digestion site (ENLYFQ, 6-aa) was inserted into the primers Lk-286TE-3R and Lk-286TE-4F by DNA synthesis. To remove the ACP-TE-linker and His tag by recombinant TEV protease, the protocol was sequentially performed by NTA-purification of recombinant TEV protease and ACP-TE-linker-TEV-286 Pim TE (311 aa), TEV digestion at 30 °C for 3 h (ratio: 5 mg TE vs 40 mg TE protein; Figure S10E), and NTA-purification to remove the recombinant TEV and His tag-linker fragment. In the final step, the digested 286 Pim TE was further purified using FPLC.

Crystallization and Structural Determination. Crystals of Pim TE without a ligand (*apo*) were obtained by sparse matrix crystallization screening using sitting-drop vapor diffusion and optimized to a precipitant solution of 0.1 M HEPES (pH 8.0), 20−25% w/v poly(ethylene glycol) 6000, and 5% v/v (±)-2-methyl-2,4-pentanediol at 20 °C (Figure S10F,G). Drops were generated by mixing 1 μL of a purified 286 Pim TE solution with 1 μL of well buffer. Cocrystallization of Pim TE with the cyclic product **4d** (*holo*) was carried out by cocrystallization of purified Pim TE protein mixed with the substrate analogue **7**. The Pim TE protein was first purified and concentrated to 13.5 mg/mL (0.44 mM) and then mixed with DMSO-dissolved compound **7** (2.2 mM). The mixture was incubated at 30 °C for 1 h and then applied to crystal screening or subpackaged into 50 μL each for storage at −80 °C. The cocrystals grew in the well buffer with 0.1 M HEPES (pH 7.5) and 1.4 M sodium citrate. All crystals were soaked in a crystallization solution containing 20% (v/v) glycerol before being frozen in liquid nitrogen.

X-ray diffraction data of *apo*-Pim TE and *holo* Pim TE were collected at the Shanghai Synchrotron Radiation Facility beamline BL19U1 and processed using the HKL2000 software package (HKL Research, Charlottesville, VA). The structure of *apo*-Pim TE was determined by molecular replacement using the Phaser MR program in CCP4 using Pik TE (PDB: 2H7X) as a search model. The structure was modeled using *Coot* and refined with REFMAC5 to a final R_{work} of 0.2041, with an R_{free} of 0.2503. The structure of *holo* Pim TE was elucidated by

https://doi.org/10.1021/acscatal.1c04991
ACS Catal. 2022, 12, 762−776

molecular replacement using *apo*-Pim TE as the searching model and refined to a final R_{work} of 0.2015, with an R_{free} of 0.2319. A summary of the crystal data collection and statistics is provided in Table S3. PyMOL was used to prepare all graphics.

Simulation System Preparation. The initial structure of Pim TE for MD simulations was obtained from the cocrystal complex of Pim TE with its cyclized macrolide product. To mimic the acyl-enzyme intermediate, a linear natural substrate (C12-COOH, **5a**) and an unnatural substrate (C12-CH_3, **5c**) were covalently bonded to the active site S138. The two complex systems were named Pim TE-**5a** and Pim TE-**5c**. The H++ (http://biophysics.cs.vt.edu/) web was used to calculate the pK_a values of the ionizable groups to determine their standard protonation states at pH 7.0. To study the recognition and catalysis processes of Pim TE, two distances d(C1-O25) and d(Nε-O25) were constrained during 5 ns MD simulations, which could capture reasonable conformations close to the cyclized state. The distances represented the nucleophilic attack of the terminal hydroxyl group of the substrates on the acyl-enzyme intermediate and the deprotonation of the substrate hydroxyl group through H-bonding with His and Asp. Finally, the representative structure from the most dominant cluster of 5 ns MD simulations was chosen to initialize later simulations in each system.

To prepare force-field parameters for the covalent substrates, an N-terminal cap(-$COCH_3$) and a C-terminal cap(-$NHCH_3$) were added to S138 to block both ends of the exposed peptide bond. Conformational optimization and electrostatic surface potential (ESP) charge calculations of covalent substrates were carried out using Gaussian09 at the level of HF/6-31g(d). Subsequently, a two-step restrained electrostatic potential (RESP) model was adopted to determine the charge distribution on the substrate.

Classical Molecular Dynamics Simulation. MD simulations were performed for the Pim TE-**5a** and Pim TE-**5c** systems using the AMBER ff14SB force field. All complexes were solvated in an octahedral box of TIP3P water molecules, with the thickness of the external water layer exceeding 10 Å, totaling 9949 water molecules in Pim TE-**5a** and 8432 water molecules in Pim TE-**5c**. In total, 13 sodium ions were added to maintain charge neutralization in both systems.

Both solvated systems were first subjected to 10 000 steps of minimization, followed by heating and equilibration cycles. In the heating cycle, the systems were gradually heated from 0 to 300 K through 25 000 iterations. After equilibration for 50 ps in the NPT ensemble, three 100 ns MD simulations (300 K, 1 atm) were conducted for each system with different random seeds. The particle mesh Ewald (PME) method was employed to account for long-range electrostatic interactions, and the SHAKE algorithm in its matrix form was used to fix bonds and angles involving hydrogen atoms. The cutoff for van der Waals interactions was set to 10.0 Å. Subsequently, the analyses of trajectories were performed using Cpptraj in Ambertools18.

Pim TE Site-Directed Mutagenesis *In Vitro*. The site-directed mutation of Pim TE was carried out by PCR using the primers listed in Table S2 and pLQ953 as a template. The PCR products were treated with *Dpn*I at 37 °C for 1 h to remove the plasmid template. The reaction mixture was purified by agarose gel electrophoresis. The mutant plasmid was recycled using a Gel Extraction Kit (D2500; Omega, Norcross, GA) and transformed into *E. coli* DH10B for verification and amplification. Finally, all plasmids constructed with mutated Pim TE coding sequences were sequenced and transformed into *E. coli* BL21(DE3) for expression and purification.

Pim TE Site-Directed Mutagenesis *In Vivo*. Pim TE site-directed mutations *in vivo* were achieved by homologous recombination of pLQ991 with the spores of *S. chattanoogensis* QZ01. The 2.35 kb and 3.10 kb homologous arms for Pim TE engineering were amplified with the primers HBmTE-LF/EcoHBmTE-LR and BspHBmTE-RF/HBmTE-RR, respectively. The ACP-TE cassette was first amplified using primers EcoACPTE-F/BspACPTE-R and cloned into pBluescript SK(+) to generate pSK-ACPTE, followed by sequencing (Figure S20A). The synonymous mutated *Kpn*I digestion site (ACCGTTCCC → AC<u>GGTACC</u>C) was introduced into pSK-ACPTE by PCR using the primers TE-*Kpn*I-F/R to generate pLQ990, which is easy for mutation screening (Figure S20B). The amplified homologous arms as well as the ACPTE fragment were ligated into pJTU1278 by Gibson assembly to generate plasmid pLQ991 for conjugation (Figures S20C and S21A,B). Synonymously mutated *Eco*RI and *Bsp*TI were introduced for mutation screening, and the mutation cassette was replaced in pLQ991. Using L170R as an example, Pim TE^{L170R} (AGCCTC → <u>TCTAGA</u>/*Xba*I) was introduced into pLQ990 by PCR using the primer L170R-F/R. Then, pLQ990-L170R was digested by *Bam*HI and *Bsp*TI to release the mutated cassette, which was further ligated into *Bam*HI- and *Bsp*TI-digested pLQ991 (Figures S20 and S21). The recombinant plasmid pLQ991 was then transferred into *E. coli* ET12567(pUZ8002) and introduced into the *pimG*-inactivation strain *S. chattanoogensis* QZ01 by intergeneric conjugation. The spores were produced on ISP2 plates for 7−9 days and then collected with 1.0 mL of TES buffer (0.01 M, pH 8.0) per plate. The spores were heat-shocked at 47 °C for 10 min and cooled with tap water. The spores were then incubated in a shaker (220 rpm, 37 °C) for 2.5 h after adding 1 mL of 2× YT buffer (1% w/v casein hydrolysate [LP0041; Oxoid, Basingstoke, U.K.] and 1% w/v yeast extract [LP0021; Oxoid]). After incubation, the spores were washed with LB once to remove buffers and resuspended in 500 μL of LB. *E. coli* ET12567 with pJTU1278-derived plasmid was cultured in 4 mL of LB with kanamycin (50 mg/mL), chloramphenicol (50 mg/mL), and ampicillin (100 mg/mL) for 3−4 h until the OD_{600} reached 0.4−0.6. *E. coli* cells (4 mL) were collected in 1 mL of LB and washed with LB broth three times to remove the antibiotics. Spores and *E. coli* cells were mixed in the ratio (spores: *E. coli* cells, v/v, μL) of 500:100, 500:200, 500:400, and 500:1000, and then cultivated on ISP2 plates with 10 mM Mg^{2+} at 30 °C for 17−19 h. The plates were then flooded with water containing 20 mg/mL thiostrepton (Thio) and 200 mg/mL trimethoprim (TMP). Exconjugants grew after 5 days and were then cultured in TSBY with 20 mg/mL Thio and 50 mg/mL TMP to obtain sufficient mycelia for sporulation and PCR verification. The positive exconjugants were further cultivated on the ISP2 medium without antibiotics for sporulation to lose the parental plasmid. Single colonies of potential Pim TE mutations were selected by dilution separation on ISP2 plates and cultivated separately in 1 mL of TSBY.

Pim TE mutations were verified using polymerase chain reaction restriction fragment length polymorphism (PCR-RFLP) maps. PCR products amplified using primers vTE-F/R and mycelia as templates were digested by restriction enzymes first and then detected by agarose gel electrophoresis (Figure S21). Since the specific restriction enzyme recognition sites

https://doi.org/10.1021/acscatal.1c04991
ACS Catal. 2022, 12, 762−776

were introduced into both sides of the Pim TE mutation site, the PCR products from target mutants were digested by restriction enzymes. PCR products using the DNA of the wild-type strain as a template were not digested. The PCR products from the exconjugants were partially digested. Moreover, using the genomic DNA extracted from mutant strains as templates, TE domains were amplified using the primer 286PTE-F/R, and target mutation sites were confirmed by sequencing (sequencing primer: Seq-TE, Figure S21C and Table S2).

■ ASSOCIATED CONTENT

Supporting Information

The Supporting Information is available free of charge at https://pubs.acs.org/doi/10.1021/acscatal.1c04991.

Strains and plasmids, primers used for TE heterologous expression and site-directed mutagenesis *in vitro* and *in vivo*, sequence information, crystal data collection and refinement statistics, thioesterase accession numbers, phylogenetic analysis, SDS-PAGE analysis of Pim TE and the crystals, schematic construction of mutant strains, MD simulation, HPLC and LC-MS profiles, and NMR data and LC-Q-TOF-MS/MS data analysis (PDF)

Detailed data and statistical analysis of *in vitro* enzymatic catalysis on Pim TE mutations (XLSX)

Titer evaluation and statistical analysis of decarboxylated pimaricin derivatives produced by Pim TE mutant strains (XLSX)

■ AUTHOR INFORMATION

Corresponding Authors

Jianting Zheng − *State Key Laboratory of Microbial Metabolism, School of Life Sciences and Biotechnology, Shanghai Jiao Tong University, Shanghai 200240, China; Joint International Research Laboratory of Metabolic and Developmental Sciences, Shanghai Jiao Tong University, Shanghai 200240, China;* orcid.org/0000-0003-1250-3556; Email: jtzheng@sjtu.edu.cn

Yilei Zhao − *State Key Laboratory of Microbial Metabolism, School of Life Sciences and Biotechnology, Shanghai Jiao Tong University, Shanghai 200240, China; Joint International Research Laboratory of Metabolic and Developmental Sciences, Shanghai Jiao Tong University, Shanghai 200240, China;* orcid.org/0000-0003-4687-7847; Email: yileizhao@sjtu.edu.cn

Linquan Bai − *State Key Laboratory of Microbial Metabolism, School of Life Sciences and Biotechnology, Shanghai Jiao Tong University, Shanghai 200240, China; Joint International Research Laboratory of Metabolic and Developmental Sciences, Shanghai Jiao Tong University, Shanghai 200240, China;* orcid.org/0000-0002-3269-9747; Email: bailq@sjtu.edu.cn

Authors

Yucong Zhou − *State Key Laboratory of Microbial Metabolism, School of Life Sciences and Biotechnology, Shanghai Jiao Tong University, Shanghai 200240, China; Joint International Research Laboratory of Metabolic and Developmental Sciences, Shanghai Jiao Tong University, Shanghai 200240, China*

Wentao Tao − *State Key Laboratory of Microbial Metabolism, School of Life Sciences and Biotechnology, Shanghai Jiao Tong University, Shanghai 200240, China; Joint International Research Laboratory of Metabolic and Developmental Sciences, Shanghai Jiao Tong University, Shanghai 200240, China*

Zhen Qi − *State Key Laboratory of Microbial Metabolism, School of Life Sciences and Biotechnology, Shanghai Jiao Tong University, Shanghai 200240, China; Joint International Research Laboratory of Metabolic and Developmental Sciences, Shanghai Jiao Tong University, Shanghai 200240, China*

Jianhua Wei − *State Key Laboratory of Microbial Metabolism, School of Life Sciences and Biotechnology, Shanghai Jiao Tong University, Shanghai 200240, China; Joint International Research Laboratory of Metabolic and Developmental Sciences, Shanghai Jiao Tong University, Shanghai 200240, China*

Ting Shi − *State Key Laboratory of Microbial Metabolism, School of Life Sciences and Biotechnology, Shanghai Jiao Tong University, Shanghai 200240, China; Joint International Research Laboratory of Metabolic and Developmental Sciences, Shanghai Jiao Tong University, Shanghai 200240, China;* orcid.org/0000-0003-3921-4412

Qianjin Kang − *State Key Laboratory of Microbial Metabolism, School of Life Sciences and Biotechnology, Shanghai Jiao Tong University, Shanghai 200240, China; Joint International Research Laboratory of Metabolic and Developmental Sciences, Shanghai Jiao Tong University, Shanghai 200240, China;* orcid.org/0000-0002-4894-0056

Complete contact information is available at: https://pubs.acs.org/10.1021/acscatal.1c04991

Author Contributions

Y.Z., T.S., J.Z., Y.Z., and L.B. designed the research; Y.Z., Q.Z., J.W., Q.K., and L.B. performed the biochemical analysis, mutagenesis *in vitro* and *vivo*, and NMR spectroscopy analysis; Y.Z., J.W., J.Z., and L.B. finished crystallization and data procession; Y.Z., W.T., T.S., Y.Z., and L.B. generated MD simulation and data analysis; and Y.Z., J.Z., T.S., Y.Z., and L.B. wrote the manuscript. All authors have given approval to the final version of the manuscript.

Funding

This work was financially supported by the National Key R&D Program of China (2021YFC2100600, 2019YFA0905400, 2018YFA0901200), the National Natural Science Foundation of China (31830104, 31801036, U1703236, 32070041, 31770070, and 31970041), and the Natural Science Foundation of Shanghai (19ZR1427300).

Notes

The authors declare no competing financial interest.

■ ACKNOWLEDGMENTS

The authors thank the staff of the BL17U, BL18U, and BL19U beamline at the Shanghai Synchrotron Radiation Facility for the crystal diffraction data acquisition and processing. They also thank the Instrumental Analysis Center of SJTU for providing services and thank Xingzhi Jiao for help with NMR data processing. They thank Dr. Wei Zhang in the Core Facilitiy and Technical Service Center for School of Life Sciences and Biotechnology, SJTU, for help with LC-Q-TOF-MS/MS data acquisition and data analysis. They also thank M.Sc. Shuobing Fan, Zeqian Du and the SJTU-HPC

computing facility award for modeling and computation. They also thank Dr. Hao Liu in the school of pharmacy, SJTU, for experimental preparation, protein purfication and fermentation.

■ ABBREVIATIONS

10-DML, 10-deoxymethynolide; ACP, acyl carrier protein; AT, acyltransferase; DH, dehydratase; ER, enoylreductase; ESI, electrospray ionization; ESP, electrostatic surface potential; HR-ESI-MS, high-resolution electrospray ionization mass spectroscopy; KR, ketoreductase; LC-Q-TOF-MS, qualitative tandem liquid chromatography quadrupole time of flight mass spectrometry; KS, ketosynthase; MD, molecular dynamics; Pik, pikromycin; Pim TE, pimaricin TE; PKS, polyketide synthase; PME, particle mesh Ewald; RESP, restrained electrostatic potential; PCR-RFLP, polymerase chain reaction restriction fragment length polymorphism; SDS-PAGE, sodium dodecyl sulfate-polyacrylamide gel electrophoresis; SNAC, *N*-acetylcysteamine; TE, thioesterase; TEV, tobacco etch virus; Thio, thiostrepton; TMC, tautomycetin; TMP, trimethoprim

■ REFERENCES

(1) Robertsen, H. L.; Musiol-Kroll, E. M. Actinomycete-derived polyketides as a source of antibiotics and lead structures for the development of new antimicrobial drugs. *Antibiotics* **2019**, *8*, No. 157.
(2) Lewis, K. The science of antibiotic discovery. *Cell* **2020**, *181*, 29−45.
(3) Castellana, M.; Wilson, M. Z.; Xu, Y.; Joshi, P.; Cristea, I. M.; Rabinowitz, J. D.; Gitai, Z.; Wingreen, N. S. Enzyme clustering accelerates processing of intermediates through metabolic channeling. *Nat. Biotechnol.* **2014**, *32*, 1011−1018.
(4) Kong, D.; Lee, M. J.; Lin, S.; Kim, E. S. Biosynthesis and pathway engineering of antifungal polyene macrolides in actinomycetes. *J. Ind. Microbiol. Biotechnol.* **2013**, *40*, 529−543.
(5) Murphy, B.; Anderson, K.; Borissow, C.; Caffrey, P.; Griffith, G.; Hearn, J.; Ibrahim, O.; Khan, N.; Lamburn, N.; Lee, M.; Pugh, K.; Rawlings, B. Isolation and characterisation of amphotericin B analogues and truncated polyketide intermediates produced by genetic engineering of *Streptomyces nodosus*. *Org. Biomol. Chem.* **2010**, *8*, 3758−3770.
(6) McDaniel, R.; Thamchaipenet, A.; Gustafsson, C.; Fu, H.; Betlach, M.; Ashley, G.; et al. Multiple genetic modifications of the erythromycin polyketide synthase to produce a library of novel "unnatural" natural products. *Proc. Natl. Acad. Sci. U.S.A.* **1999**, *96*, 1846−1851.
(7) Nivina, A.; Yuet, K. P.; Hsu, J.; Khosla, C. Evolution and diversity of assembly-line polyketide synthases. *Chem. Rev.* **2019**, *119*, 12524−12547.
(8) Tsai, S. C.; Miercke, L. J.; Krucinski, J.; Gokhale, R.; Chen, J. C.; Foster, P. G.; Cane, D. E.; Khosla, C.; Stroud, R. M. Crystal structure of the macrocycle-forming thioesterase domain of the erythromycin polyketide synthase: versatility from a unique substrate channel. *Proc. Natl. Acad. Sci. U.S.A.* **2001**, *98*, 14808−14813.
(9) Yoon, Y. J.; Kim, E. S.; Hwang, Y. S.; Choi, C. Y. Avermectin: biochemical and molecular basis of its biosynthesis and regulation. *Appl. Microbiol. Biotechnol.* **2004**, *63*, 626−634.
(10) Caffrey, P.; Lynch, S.; Flood, E.; Finnan, S.; Oliynyk, M. Amphotericin biosynthesis in *Streptomyces nodosus*: deductions from analysis of polyketide synthase and late genes. *Chem. Biol.* **2001**, *8*, 713−723.
(11) Horsman, M. E.; Hari, T. P.; Boddy, C. N. Polyketide synthase and non-ribosomal peptide synthetase thioesterase selectivity: logic gate or a victim of fate? *Nat. Prod. Rep.* **2016**, *33*, 183−202.
(12) Tsai, S. C.; Lu, H.; Cane, D. E.; Khosla, C.; Stroud, R. M. Insights into channel architecture and substrate specificity from crystal structures of two macrocycle-forming thioesterases of modular polyketide synthases. *Biochemistry* **2002**, *41*, 12598−12606.
(13) Giraldes, J. W.; Akey, D. L.; Kittendorf, J. D.; Sherman, D. H.; Smith, J. L.; Fecik, R. A. Structural and mechanistic insights into polyketide macrolactonization from polyketide-based affinity labels. *Nat. Chem. Biol.* **2006**, *2*, 531−536.
(14) Akey, D. L.; Kittendorf, J. D.; Giraldes, J. W.; Fecik, R. A.; Sherman, D. H.; Smith, J. L. Structural basis for macrolactonization by the pikromycin thioesterase. *Nat. Chem. Biol.* **2006**, *2*, 537−542.
(15) Shi, T.; Liu, L.; Tao, W.; Luo, S.; Fan, S.; Wang, X.; Bai, L.; Zhao, Y. Theoretical studies on the catalytic mechanism and substrate diversity for macrocyclization of pikromycin thioesterase. *ACS Catal.* **2018**, *8*, 4323−4332.
(16) Chen, X.; Shi, T.; Wang, X.; Wang, J.; Chen, Q.; Bai, L.; Zhao, Y. Theoretical studies on the mechanism of thioesterase-catalyzed macrocyclization in erythromycin biosynthesis. *ACS Catal.* **2016**, *6*, 4369−4378.
(17) Koch, A. A.; Hansen, D. A.; Shende, V. V.; Furan, L. R.; Houk, K. N.; Jimenez-Oses, G.; Sherman, D. H. A single active site mutation in the pikromycin thioesterase generates a more effective macrocyclization catalyst. *J. Am. Chem. Soc.* **2017**, *139*, 13456−13465.
(18) Santos-Aberturas, J.; Engel, J.; Dickerhoff, J.; Dörr, M.; Rudroff, F.; Weisz, K.; Bornscheuer, U. T. Exploration of the substrate promiscuity of biosynthetic tailoring enzymes as a new source of structural diversity for polyene macrolide antifungals. *ChemCatChem* **2015**, *7*, 490−500.
(19) Kells, P. M.; Ouellet, H.; Santos-Aberturas, J.; Aparicio, J. F.; Podust, L. M. Structure of cytochrome P450 PimD suggests epoxidation of the polyene macrolide pimaricin occurs via a hydroperoxoferric intermediate. *Chem. Biol.* **2010**, *17*, 841−851.
(20) Hutchinson, E.; Murphy, B.; Dunne, T.; Breen, C.; Rawlings, B.; Caffrey, P. Redesign of polyene macrolide glycosylation: engineered biosynthesis of 19-(O)-perosaminyl-amphoteronolide B. *Chem. Biol.* **2010**, *17*, 174−182.
(21) Brautaset, T.; Sletta, H.; Nedal, A.; Borgos, S. E.; Degnes, K. F.; Bakke, I.; Volokhan, O.; Sekurova, O. N.; Treshalin, I. D.; Mirchink, E. P.; Dikiy, A.; Ellingsen, T. E.; Zotchev, S. B. Improved antifungal polyene macrolides *via* engineering of the nystatin biosynthetic genes in *Streptomyces noursei*. *Chem. Biol.* **2008**, *15*, 1198−1206.
(22) Davis, S. A.; Vincent, B. M.; Endo, M. M.; Whitesell, L.; Marchillo, K.; Andes, D. R.; Lindquist, S.; Burke, M. D. Nontoxic antimicrobials that evade drug resistance. *Nat. Chem. Biol.* **2015**, *11*, 481−487.
(23) Aparicio, J. F.; Barreales, E. G.; Payero, T. D.; Vicente, C. M.; de Pedro, A.; Santos-Aberturas, J. Biotechnological production and application of the antibiotic pimaricin: biosynthesis and its regulation. *Appl. Microbiol. Biotechnol.* **2016**, *100*, 61−78.
(24) Carmody, M.; Murphy, B.; Byrne, B.; Power, P.; Rai, D.; Rawlings, B.; Caffrey, P. Biosynthesis of amphotericin derivatives lacking exocyclic carboxyl groups. *J. Biol. Chem.* **2005**, *280*, 34420−34426.
(25) Seco, E. M.; Fotso, S.; Laatsch, H.; Malpartida, F. A tailoring activity is responsible for generating polyene amide derivatives in *Streptomyces diastaticus* var. 108. *Chem. Biol.* **2005**, *12*, 1093−1101.
(26) Chen, S.; Mao, X.; Shen, Y.; Zhou, Y.; Li, J.; Wang, L.; Tao, X.; Yang, L.; Wang, Y.; Zhou, X.; Deng, Z.; Wei, D. Tailoring the P450 monooxygenase gene for FR-008/candicidin biosynthesis. *Appl. Environ. Microbiol.* **2009**, *75*, 1778−1781.
(27) Brautaset, T.; Sletta, H.; Degnes, K. F.; Sekurova, O. N.; Bakke, I.; Volokhan, O.; Andreassen, T.; Ellingsen, T. E.; Zotchev, S. B. New nystatin-related antifungal polyene macrolides with altered polyol region generated via biosynthetic engineering of *Streptomyces noursei*. *Appl. Environ. Microbiol.* **2011**, *77*, 6636−6643.
(28) Qi, Z.; Kang, Q.; Jiang, C.; Han, M.; Bai, L. Engineered biosynthesis of pimaricin derivatives with improved antifungal activity and reduced cytotoxicity. *Appl. Microbiol. Biotechnol.* **2015**, *99*, 6745−6752.
(29) Qi, Z.; Zhou, Y.; Kang, Q.; Jiang, C.; Zheng, J.; Bai, L. Directed accumulation of less toxic pimaricin derivatives by improving the efficiency of a polyketide synthase dehydratase domain. *Appl. Microbiol. Biotechnol.* **2017**, *101*, 2427−2436.

https://doi.org/10.1021/acscatal.1c04991
ACS Catal. 2022, 12, 762−776

(30) Hansen, D. A.; Koch, A. A.; Sherman, D. H. Identification of a thioesterase bottleneck in the pikromycin pathway through full-module processing of unnatural pentaketides. *J. Am. Chem. Soc.* **2017**, *139*, 13450−13455.
(31) Koch, A. A.; Schmidt, J. J.; Lowell, A. N.; Hansen, D. A.; Coburn, K. M.; Chemler, J. A.; Sherman, D. H. Probing selectivity and creating structural diversity through hybrid polyketide synthases. *Angew. Chem., Int. Ed.* **2020**, *59*, 13575−13580.
(32) Tripathi, A.; Choi, S. S.; Sherman, D. H.; Kim, E. S. Thioesterase domain swapping of a linear polyketide tautomycetin with a macrocyclic polyketide pikromycin in *Streptomyces* sp. CK4412. *J. Ind. Microbiol. Biotechnol.* **2016**, *43*, 1189−1193.
(33) Scaglione, J. B.; Akey, D. L.; Sullivan, R.; Kittendorf, J. D.; Rath, C. M.; Kim, E. S.; Smith, J. L.; Sherman, D. H. Biochemical and structural characterization of the tautomycetin thioesterase: analysis of a stereoselective polyketide hydrolase. *Angew. Chem., Int. Ed.* **2010**, *49*, 5726−5730.
(34) Wang, Y.; Xue, P.; Cao, M.; Yu, T.; Lane, S. T.; Zhao, H. Directed evolution: methodologies and applications. *Chem. Rev.* **2021**, *121*, 12384−12444.

https://doi.org/10.1021/acscatal.1c04991
ACS Catal. 2022, 12, 762−776